Electronic Supplementary Material (ESI) for Organic Chemistry Frontiers.

Supporting Information

In situ fluorescence visualizing of temperature-dependent photoreaction process of pyridazine *N*-oxide

Jianye Gong,[‡a] Junyi Gong,[‡b] Yumao He,[a] Chunbin Li,[a] Bo Yang,[a] Lingxiu Liu,[a] Guoyu Jiang,*[a] and Jianguo Wang*[a]

[a]College of Chemistry and Chemical Engineering, Inner Mongolia Key Laboratory of Fine Organic Synthesis, Inner Mongolia University, Hohhot 010021, P. R. China.

E-mail: jiangguoyu@mail.ipc.ac.cn; wangjg@iccas.ac.cn

[b]School of Science and Engineering, Shenzhen Institute of Aggregate Science and Technology, The Chinese University of Hong Kong, Shenzhen, Guangdong 518172, P. R. China.

Table of Contents

1. Materials and instruments

N,N-diphenyl-4-(4,4,5,5-tetramethyl-1,3,2-dioxaborolan-2-yl)aniline were purchased from Soochiral chemistry. 3,6-Dichloropyridazine and morpholine were purchased from Innochem. All other chemicals and reagents were purchased from Admas-beta® and used directly without further purification. ^{1}H and ^{13}C NMR spectra were recorded with a Bruker ARX 500 NMR spectrometer using tetramethylsilane (TMS) as a reference. High resolution mass spectra (HRMS) were measured with a LCMS9030 spectrometer. UV-vis absorption spectra were recorded on a SHIMADZU UV-2600i spectrophotometer. Photoluminescence (PL) spectra were recorded on a HITACHI F-4700 fluorescence spectrophotometer. The absolute fluorescence quantum yield was measured using a Hamamatsu quantum yield spectrometer C11347-11 Quantaurus QY. Single crystal X-ray diffraction was performed on a Rigaku Oxford Diffraction Supernova Dual Source, Cu at Zero equipped with an AtlasS2 CCD using Cu Kα radiation. The data were collected and processed using CrysAlisPro.

2. Theoretical calculations

In calculation of Gibbs free energy, the theoretical ground-state geometry and electronic structure of molecules were optimized using the density functional theory (DFT) at B3LYP/def2-SVP with program ORCA[1]. The HOMO and LUMO electron cloud distribution of MPZ and MPD-O in crystal were calculated at the level of B3LYP/6-311+G(d). The geometry of *trans*-MDO was optimized using B3LYP/6-311+G(d). All the theoretical calculations were performed using Gaussian 09 package.

3. Synthesis and characterization

Synthesis of MPD-O: MPD-O was synthesized according to the literature method. [2]

Photosynthesis of MPZ: To a 50 mL round-bottom flask was added MPD-O (106 mg, 0.25 mmol) dissolved in THF (5 mL). The resulting solution was stirred under irradiation from a 365 nm hand-held UV lamp for 3 h at room temperature for complete reaction. The resulting solution was concentrated under reduced pressure. The yellow residue was washed with CH_2Cl_2 (3 mL). The resulting suspension was filtered to afford the title compound (81 mg, 76% yield) as a colorless powder. ^{1}H NMR (500 MHz, $CDCl_3$), δ (ppm): 7.54 (d, J = 8.5 Hz, 2H), 7.30 (t, J = 8.4 Hz, 4H), 7.13 (t, J = 7.6 Hz, 6H), 7.08 (t, J = 7.4 Hz, 2H), 6.93 (s, 1H), 4.06 (s, 2H), 3.84 (s, 2H), 3.79 (s, 4H); ^{13}C NMR (126 MHz, $CDCl_3$), δ (ppm): 161.75, 148.37, 147.31, 146.95, 129.41, 126.48, 124.79, 123.67, 123.44, 123.20, 104.18, 66.95, 47.59, 42.94; HRMS (ESI): *m*/*z:* $[M+H]^+$ calcd for $[C_{26}H_{25}N_4O_2]^+$: 425.19775; found: 425.19720.

Photosynthesis of *trans*-MDO: To a 50 mL round-bottom flask was added MPD-O (43 mg, 0.1 mmol) dissolved in freshly distilled THF (5 mL). The resulting solution was stirred under irradiation from a 365 nm hand-held UV lamp for 4 d at -40 ℃ for complete reaction. The resulting solution was concentrated under reduced pressure. The crude product was purified by silica gel column chromatography using petroleum ether/ethyl acetate (*v*:*v*, 1:1) as an eluent to afford the title compound (26 mg, 63% yield) as a yellow powder. ^{1}H NMR (500 MHz, THF-d_8), δ (ppm): 7.92 – 7.88 (m, 3H), 7.44 (d, J = 14.9 Hz, 1H), 7.32 (t, J = 8.4 Hz, 4H), 7.16 – 7.12 (m, 6H), 6.99 (d, J = 8.9 Hz, 2H), 3.61 (s, 8H); ^{13}C NMR (126 MHz, THF-d_8), δ (ppm): 184.12, 161.43, 150.57, 144.65, 132.00, 129.17, 128.31, 127.98, 127.65, 124.14, 122.81, 117.51, 44.23, 40.34; HRMS (ESI): *m*/*z:* $[M+H]^+$ calcd for $[C_{26}H_{25}N_2O_3]^+$: 413.18652; found: 413.18597.

cis-MDO: ^{1}H NMR (500 MHz, $CDCl_3$), δ (ppm): 7.82 (d, J = 9.0 Hz, 2H), 7.35 (t, J = 7.7 Hz, 4H), 7.19 – 7.17 (m, 6H), 7.00 (t, J = 8.8 Hz, 2H), 6.52 (d, J = 12.0 Hz, 1H), 3.76 (s, 2H), 3.71 (s, 4H), 3.49 (s, 2H); HRMS (ESI): *m*/*z:* $[M+H]^+$ calcd for $[C_{26}H_{25}N_2O_3]^+$: 413.18652; found: 413.18759.

Photosynthesis of MF: Following same procedure of *trans*-MDO, but resulting

solution was stirred under an atmosphere of N_2 and irradiated for 40 h at -40 °C. ^{1}H NMR (500 MHz, $CDCl_3$), δ (ppm): 7.44 (d, J = 8.5 Hz, 2H), 7.29 – 7.26 (m, 4H), 7.13 (d, J = 7.7 Hz, 4H), 7.08 (d, J = 8.7 Hz, 2H), 7.04 (t, J = 7.4 Hz, 2H), 6.48 (d, J = 3.3 Hz, 1H), 5.29 (d, J = 2.8 Hz, 1H), 3.88 (t, J = 4.8 Hz, 4H), 3.20 (t, J = 4.3 Hz, 4H); HRMS (ESI): *m/z:* $[M+H]^+$ calcd for $[C_{26}H_{25}N_2O_2]^+$: 397.19160; found: 397.19105.

4. Supplementary Figures

Table S1. Photophysical Properties of MPD-O, MPZ and *trans*-MDO.

	λ_{abs} (nm)	λ_{em} (nm)		Φ_f[a] (%)			τ_f (ns)	$k_{f,r}$[c] (s^{-1})
	Solution	Solution	Solid	Solution	Solid	α_{AIE}[b]	Solution	Solution
MPD-O	388	464	464	1.1	0.8	0.73	0.67	1.64×10^7
MPZ	324	391	407	33.1	9.2	0.28	1.72	1.92×10^8
***trans*-MDO**	392	578	547	5.3	11.8	2.23	1.48	3.58×10^7

[a] Φ_f = fluorescence quantum yield measured by using an integrating sphere

[b] $\alpha_{AIE} = \Phi_{f,solid} / \Phi_{f,solution}$

[c] $k_{f,r} = \Phi_f / \tau_f$

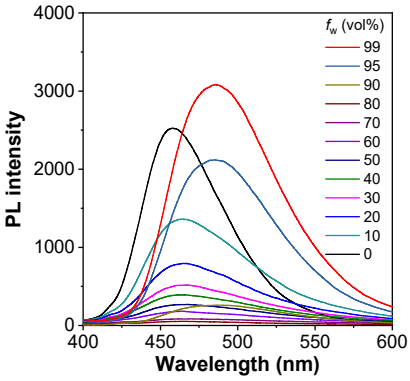

Figure S1. PL spectra of MPD-O in THF/water mixtures with different water fractions (f_w).

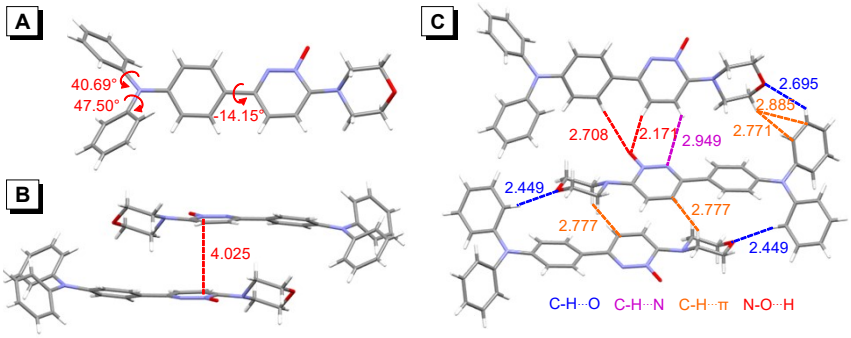

Figure S2. (A) The torsion angles in the MPD-O single crystal. (B) The distance between the two adjacent pyridazine *N*-oxide rings. (C) Intermolecular interactions of MPD-O.

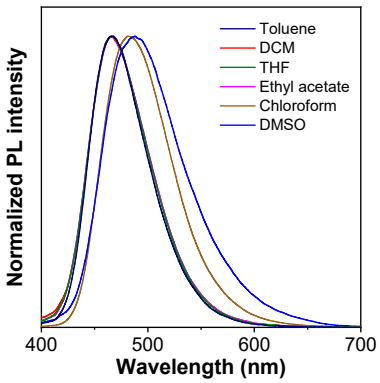

Figure S3. Normalized PL spectra of MPD-O in different solvents.

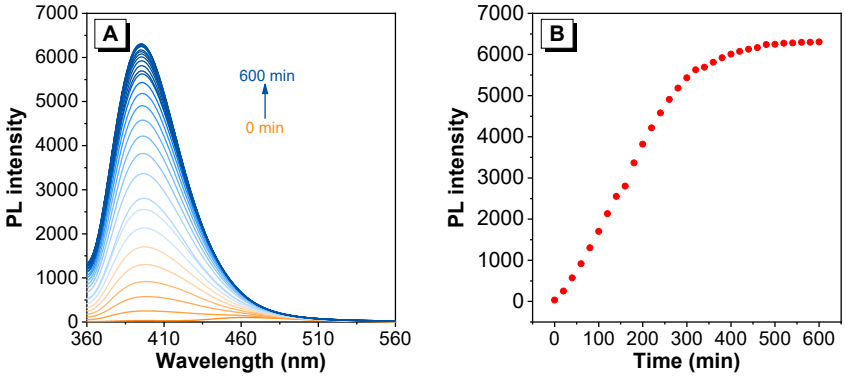

Figure S4. (A) PL spectra of MPD-O after different time of UV irradiation by the xenon lamp of the fluorescence spectrometer at room temperature. (B) Plot of the PL intensity at 395 nm versus irradiation time.

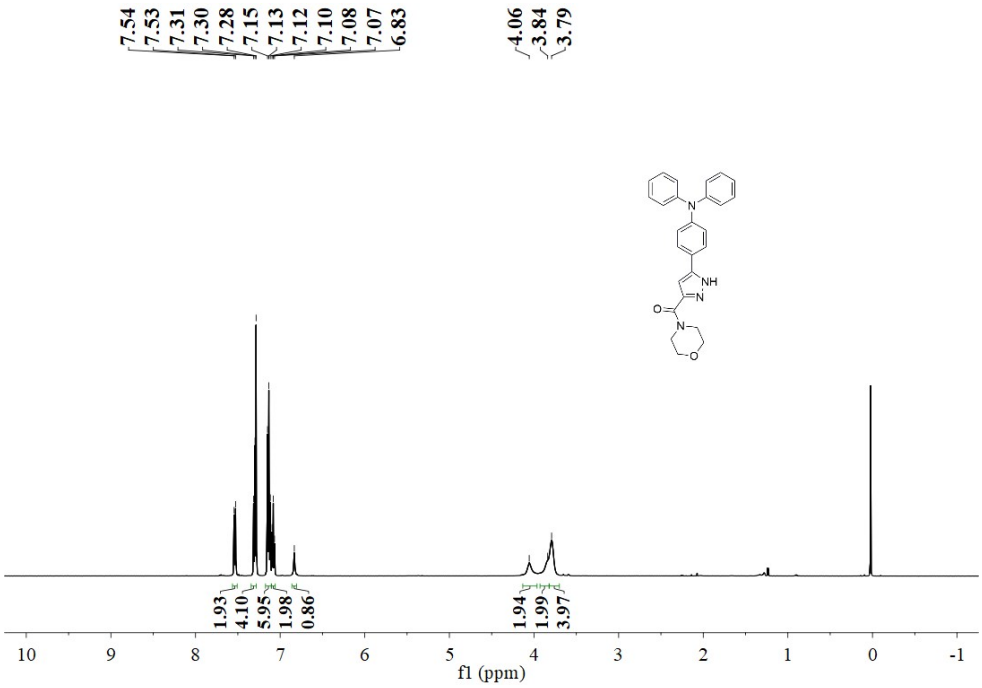

Figure S5. ^{1}H NMR spectrum of MPZ in $CDCl_3$.

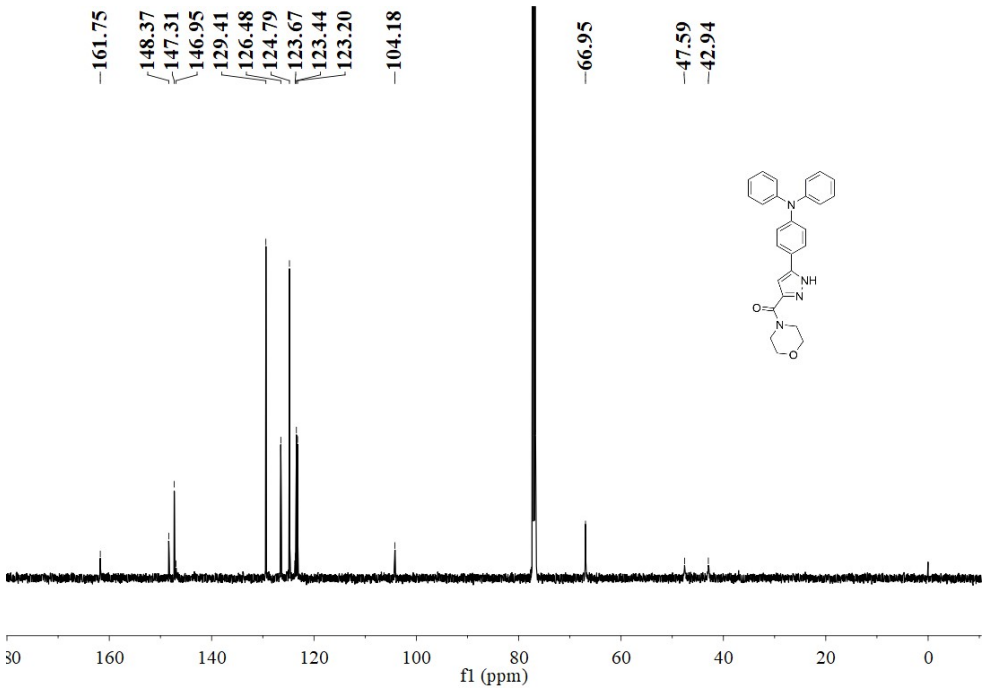

Figure S6. ^{13}C NMR spectrum of MPZ in $CDCl_3$.

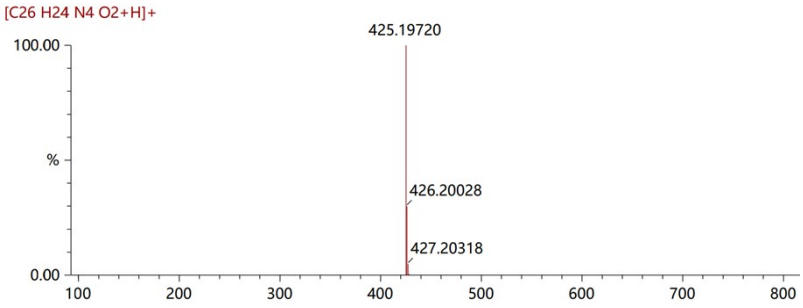

Figure S7. HRMS spectrum of MPZ.

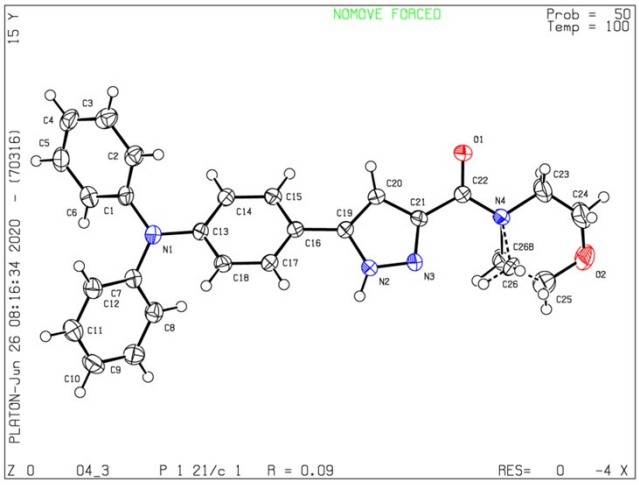

Figure S8. Single structure of MPZ.

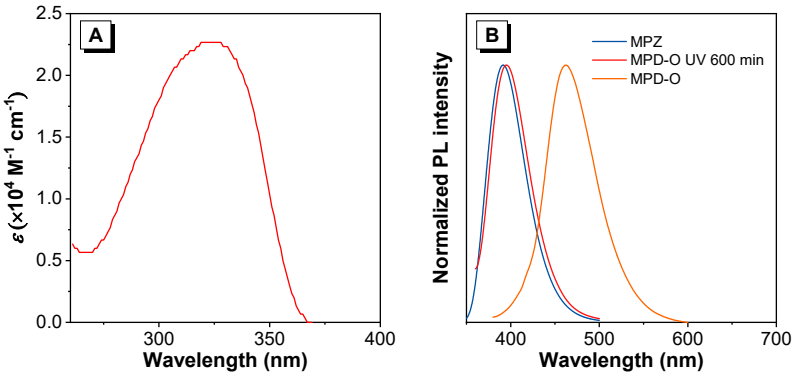

Figure S9. (A) Molar extinction coefficient of MPZ in THF (30 μM). (B) Normalized PL spectra of MPZ, MPD-O and MPD-O after UV irradiation 600 min.

Table S2. Crystallographic and structural refinement data of MPZ.

Name	MPZ
Empirical formula	$C_{26}H_{24}N_4O_2$
Formula weight	424.49
Temperature (K)	100.0(3)
Wavelength (Å)	1.54184
Crystal system	monoclinic
Space group	$P2_1/c$
a (Å)	21.4658(15)
b (Å)	11.4890(6)
c (Å)	8.7489(5)
α (°)	90
β (°)	95.255(6)
γ (°)	90
Volume (Å^3)	2148.6(2)
Z	4
2Θ range for data collection (°)	4.134 to 146.896
Index ranges	$-26 \le h \le 25$, $-14 \le k \le 9$, $-10 \le l \le 8$
CCDC Number	2210453

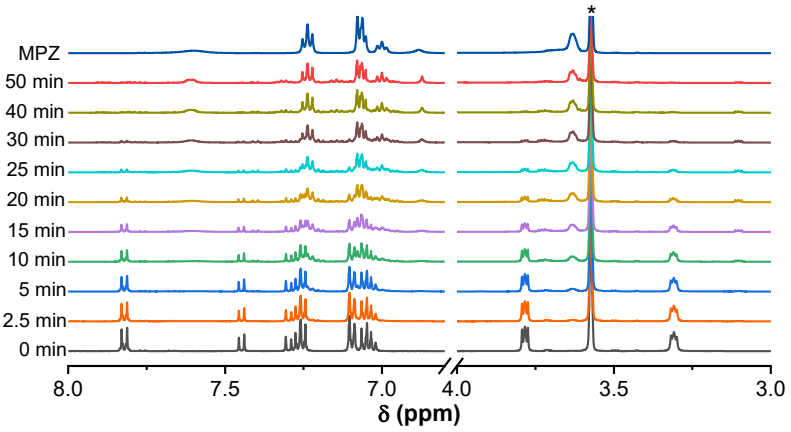

Figure S10. ^{1}H NMR spectrum of MPD-O in THF-d_8 at different time of UV irradiation by a hand-held UV lamp at room temperature.

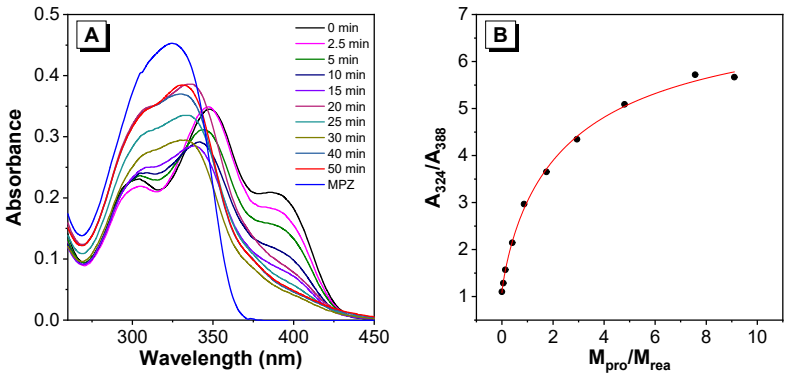

Figure S11. (A) UV-vis absorption spectra of MPD-O in THF at different irradiation time points. (B) The functional relationship between the absorbance ratio (A_{324}/A_{388}) and the molar ratio of product (M_{pro}) versus reactant (M_{rea}) calculated from ^{1}H NMR data. $Y = 7.411 - 6.33/(1 + (X/2.61)^{0.85})$, $R^2 = 0.997$.

Table S3. The molar ratio of the reaction product (M_{pro}) to the reactant (M_{rea}) was calculated based on ^{1}H NMR at different reaction times. M_{pro}/M_{rea} = integral of 7.649 – 7.563 ppm of product / integral of 7.839 – 7.800 ppm of reactant.

Time (min)	0	2.5	5	10	15	20	25	30	40	50
M_{pro}/M_{rea}	0	0.005	0.135	0.405	0.870	1.745	2.940	4.805	7.570	9.015

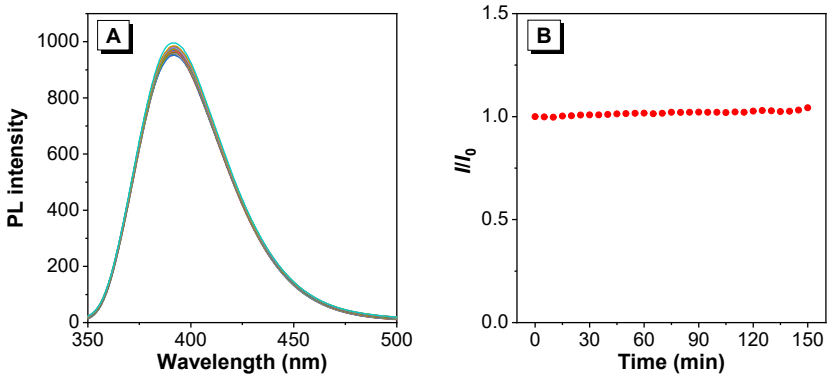

Figure S12. (A) Photostability of MPZ in THF. (B) Plot of the relative emission intensity (I/I_0) versus irradiation time.

Table S4. The corresponding CIE coordinates of MPD-O at different time in the photoreaction at low temperature of -40 °C.

Time (min)	CIE coordinate	Time (min)	CIE coordinate
0	(0.186, 0.203)	12	(0.193, 0.173)
2	(0.158, 0.041)	14	(0.205, 0.216)
4	(0.160, 0.053)	16	(0.219, 0.267)
6	(0.164, 0.068)	18	(0.232, 0.306)
8	(0.170, 0.091)	20	(0.242, 0.338)
10	(0.177, 0.116)	22	(0.247, 0.354)

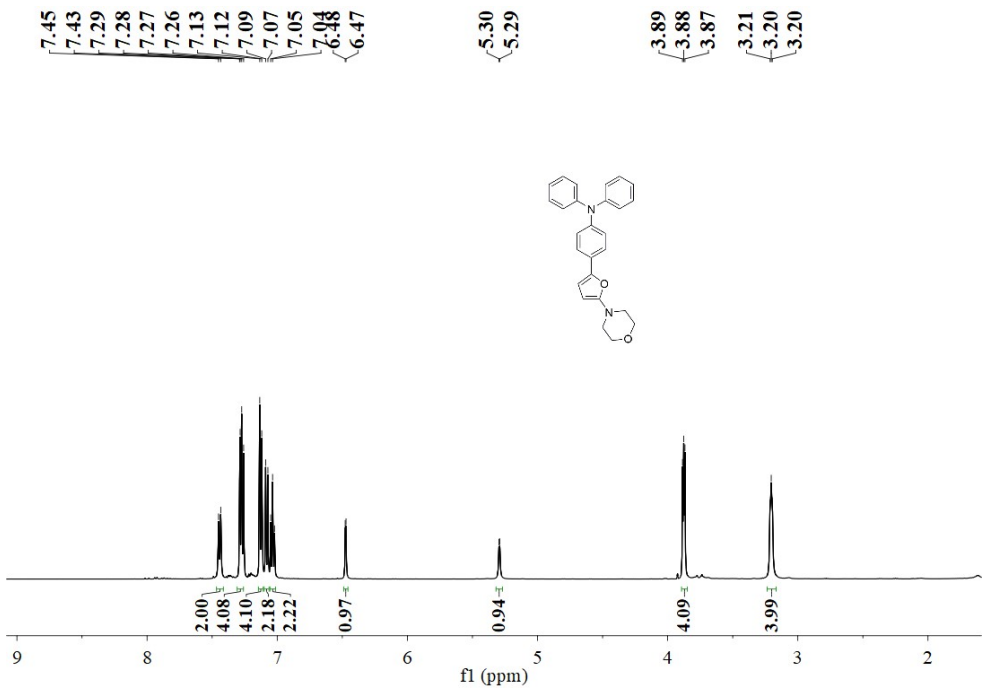

Figure S13. ^{1}H NMR spectrum of MF in $CDCl_3$.

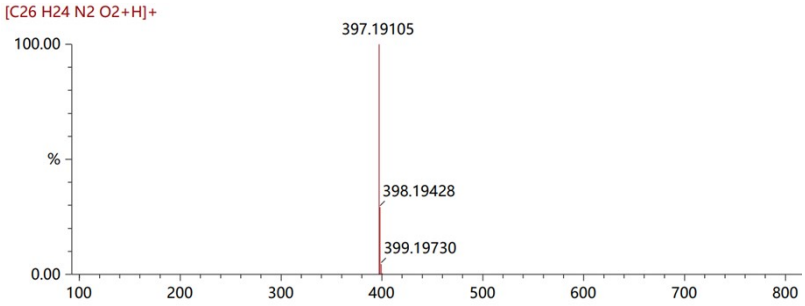

Figure S14. HRMS spectrum of MF.

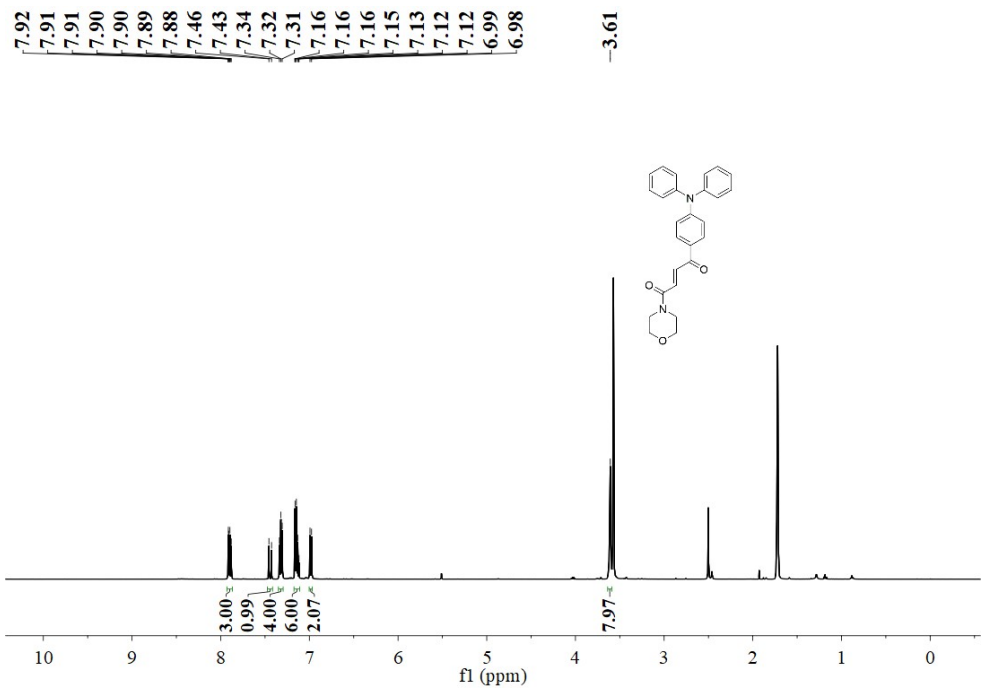

Figure S15. ^{1}H NMR spectrum of *trans*-MDO in THF-d_8.

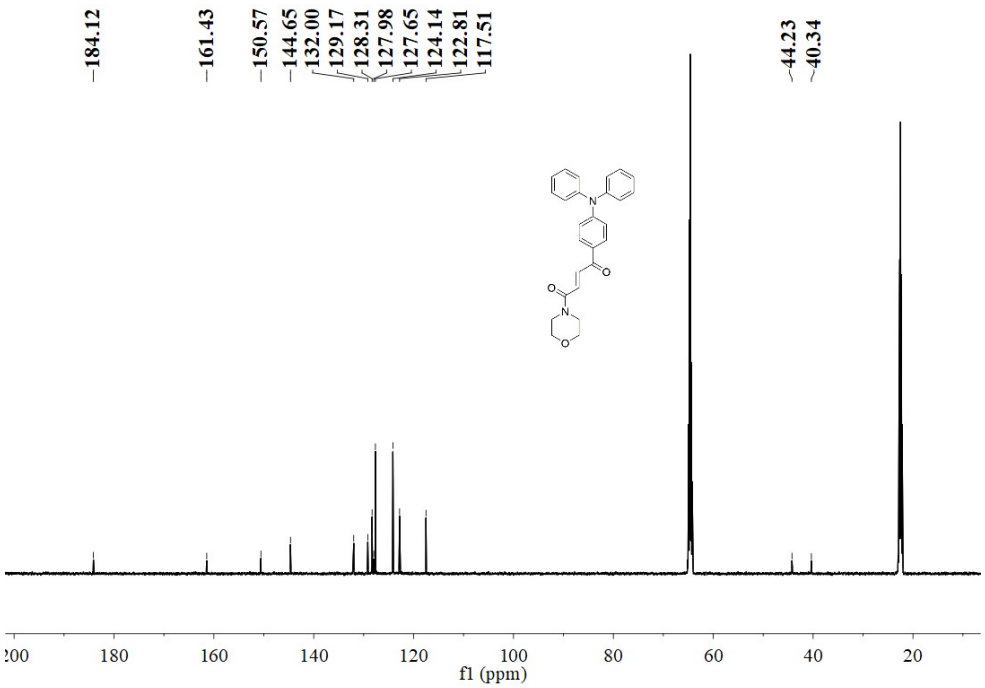

Figure S16. ^{13}C NMR spectrum of *trans*-MDO in THF-d_8.

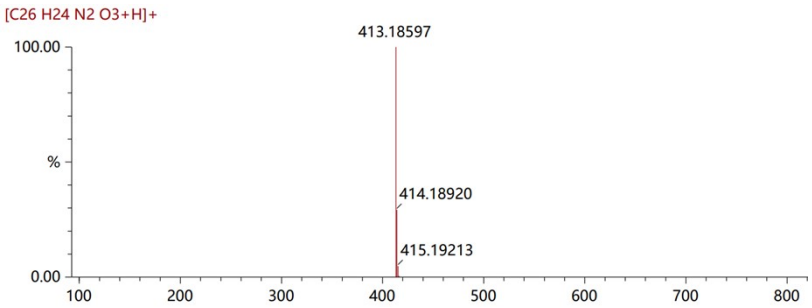

Figure S17. HRMS spectrum of *trans*-MDO.

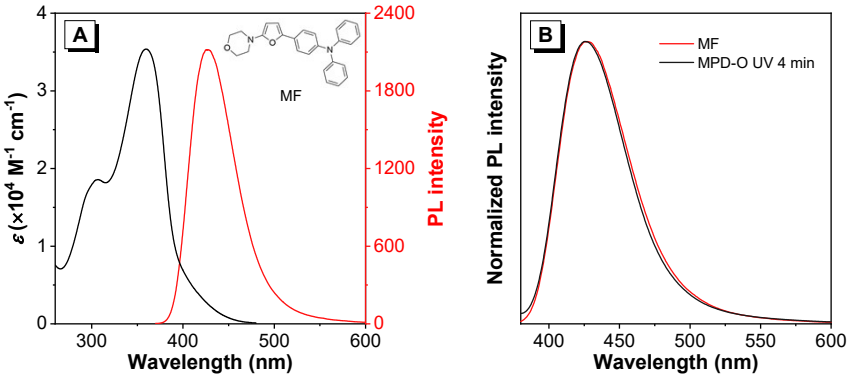

Figure S18. (A) Molar extinction coefficient and PL spectra of MF (30 μM) in THF. Inset: the structure of MF. (B) Normalized PL spectra of MF and MPD-O after UV irradiation of 4 min.

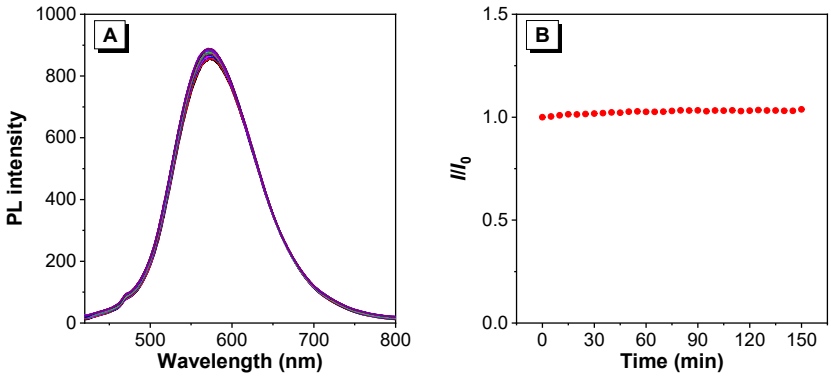

Figure S19. (A) Photostability of *trans*-MDO in THF. (B) Plot of the relative emission intensity (I/I_0) versus irradiation time.

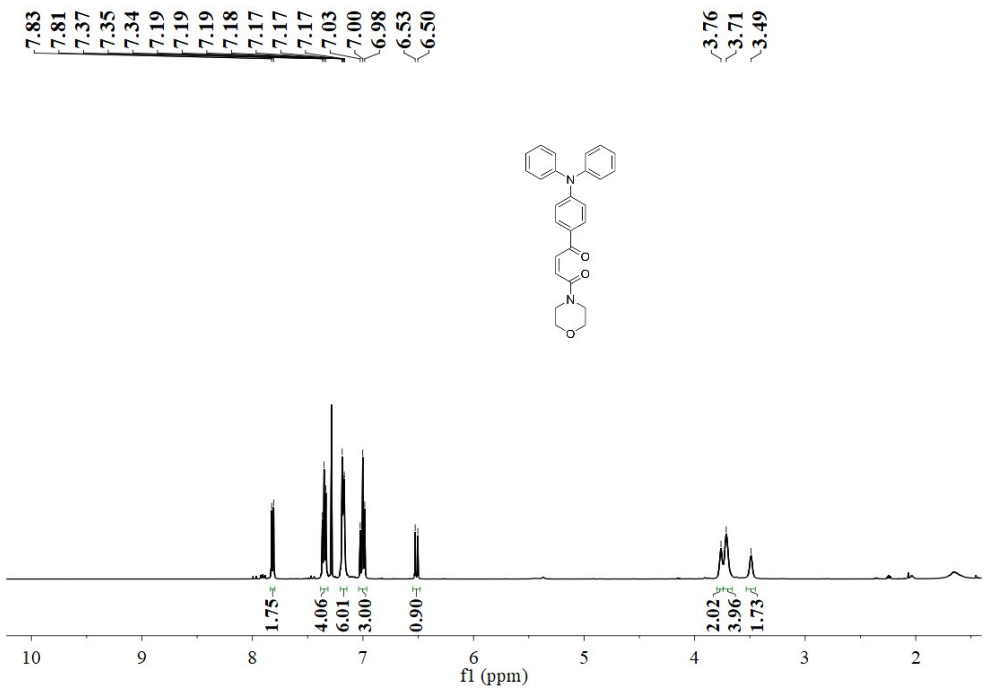

Figure S20. ^{1}H NMR spectrum of *cis*-MDO in $CDCl_3$.

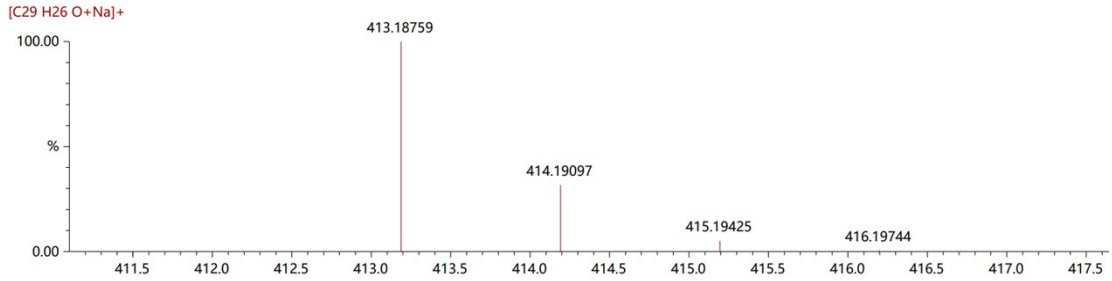

Figure S21. HRMS spectrum of *cis*-MDO.

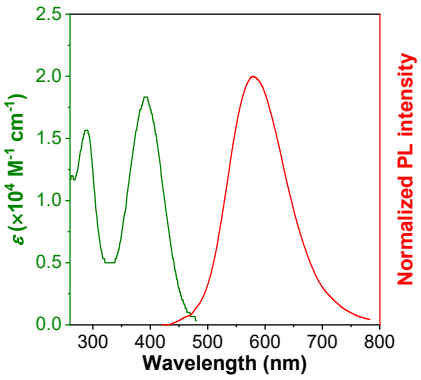

Figure S22. Molar extinction coefficient and PL spectra of *trans*-MDO (30 μM) in THF solution.

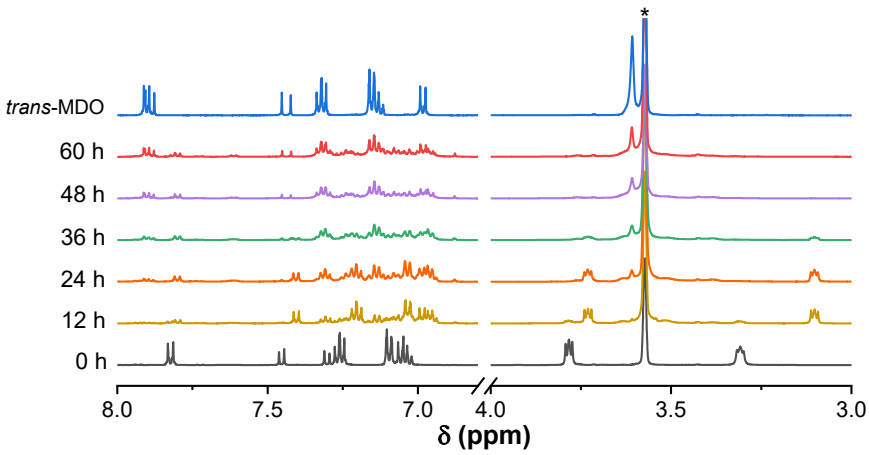

Figure S23. ^{1}H NMR spectra of MPD-O in THF-d_8 at different time of UV irradiation by a hand-held UV lamp at -40 ℃.

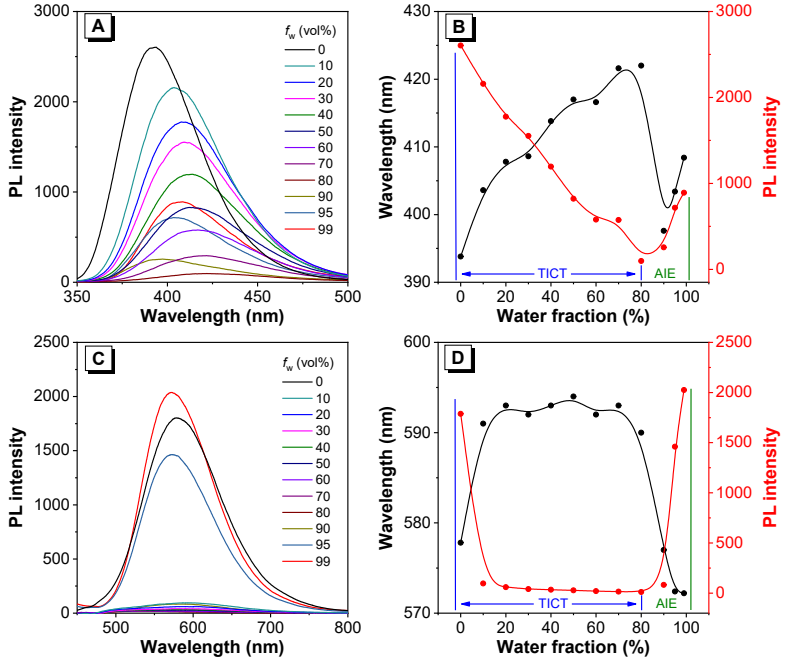

Figure S24. PL spectra of MPZ (A) and *trans*-MDO (C) in THF/water mixtures with different water fractions (f_w). Plot of maximal emission wavelength and PL intensity of MPZ (B) and *trans*-MDO (D) versus the water fraction in the THF/water mixtures.

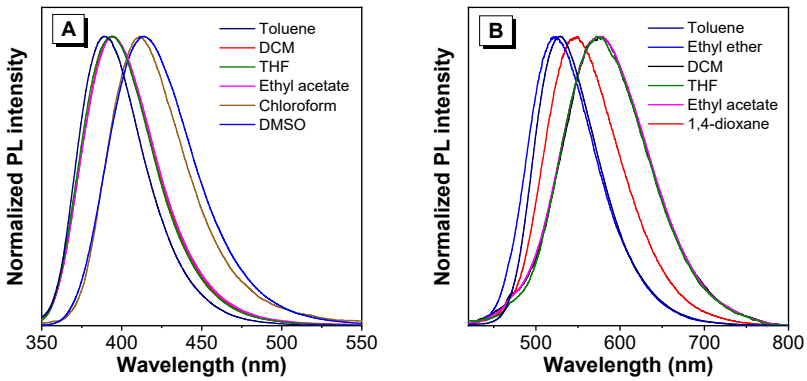

Figure S25. Normalized PL spectra of MPZ (A) and *trans*-MDO (B) in different solvents.

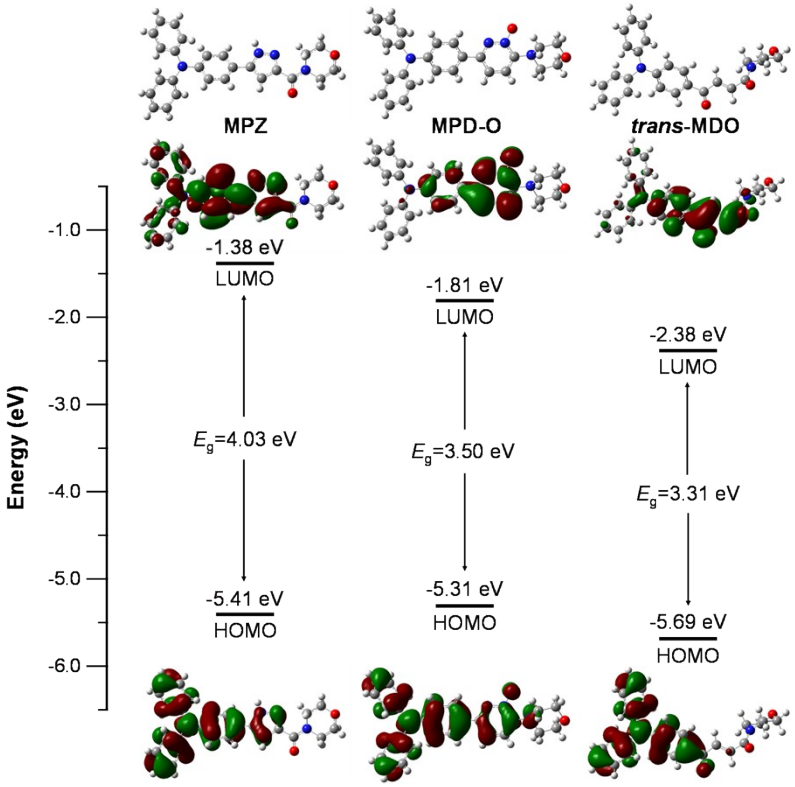

Figure S26. The HOMO and LUMO electron cloud distribution of MPZ, MPD-O, and *trans*-MDO.

5. Reference

1. F. Neese, The ORCA program system. *Wiley Interdiscip. Rev.: Comput. Mol. Sci.* 2012, **2**, 73.

2. J. Gong, L. Liu, C. Li, Y. He, J. Yu, Y. Zhang, L. Feng, G. Jiang, J. Wang and B. Z. Tang, Oxidization enhances type I ROS generation of AIE-active zwitterionic photosensitizers for photodynamic killing of drug-resistant bacteria, *Chem. Sci.*, 2023, **14**, 4863-4871.